Commun. Math. Phys. 121, 225–254 (1989)

Communications in Mathematical Physics

Complex Universality

Predrag Cvitanović and Jan Myrheim

Nordita, Blegdamsvej 17, DK-2100 Copenhagen Ø, Denmark

Abstract. The theory of period doublings for one-parameter families of iterated real mappings is generalized to period n-tuplings for complex mappings. An n-tupling occurs when the eigenvalue of a stable periodic orbit passes through the value $\omega = \exp(2\pi i m/n)$ as the parameter value is changed. Each choice of m defines a different sequence of n-tuplings, for which we construct a period n-tupling renormalization operator with a universal fixpoint function, a universal unstable manifold and universal scaling numbers. These scaling numbers can be organized by Farey trees. The present paper gives a general description and numerical support for the universality conjectured above.

Introduction

In this article we develop in some detail the generalization of the period-doubling universality for real mappings [1, 2] to the complex case. This universality was discovered by Goldberg et al. [3] and by us [4]. The conjecture is that the fixed points of period n-tupling operators associated with infinite sequences of m/n period n-tuplings of complex mappings with quadratic critical points are universal and that each such "m/n" renormalization operator has a single unstable eigenvalue $\delta_{m/n}$. Furthermore, we show that the infinity of universal scaling numbers so obtained can be organized by the underlying number-theoretic Farey trees, and that the space and parameter scaling numbers $\alpha_{m/n}$ and $\delta_{m/n}$ have well defined $n \to \infty$ limits. For example, the Feigenbaum number $\delta = 4.66\ldots$ can be interpreted as the $n=2$ case of the asymptotic estimate $|\delta_{1/n}| = n^2$. There exist a large mathematical literature on iterations of complex functions, some of which we review in Sect. 1. The difference between the present investigation (together with [3, 5, 6]), and the previous work is that we concentrate on the metric properties of complex iterations, rather than on their topological and analytic structure.

The period n-tuplings that we study here are a direct generalization of the period-doubling phenomenon known from one-dimensional real unimodal

mappings (period doublings are reviewed in [7–11]). A complex function can be viewed as a two-dimensional mapping, and iterative two-dimensional mappings are important tools for modeling dynamical systems [12, 13]. Period n-tuplings are also common in hamiltonian systems [14] and for coupled non-linear oscillators [15, 16], and, at least for the hamiltonian mappings, sequences of period n-tuplings exhibit universal scalings [14, 17]. There are further striking similarities between universal scaling behavior of circle maps [18–20] and the universality for complex maps discussed here, such as their organization by the Farey sequences (Sect. 7). At first sight, one could think that the area preserving. Hamiltonian mappings present the same universality as the (angle preserving) complex mappings discussed here. However, we argue in Sect. 2 that analytic mappings viewed as two-dimensional mappings are atypical (unless they arise from some particular physical situation [21]), and that we do not expect our universal numbers to characterize the general two-dimensional case.

1. Complex Iterations – A Brief Review

In this paper we shall study metric properties (both in iteration and parameter space) of the asymptotic iterates of

$$z_{n+1} = f(z_n), \tag{1.1}$$

where $f(z)$ is an analytic function in the complex variable z with a quadratic critical point z_c, i.e., a power series expansion of the form

$$f(z) = a_0 + a_2(z - z_c)^2 + \ldots, \qquad a_2 \neq 0. \tag{1.2}$$

Typical model mappings of this type are the Fatou [22] mapping

$$f(z) = p + z^2 \tag{1.3}$$

and the Julia [23] mapping

$$f(z) = \lambda z(1 - z). \tag{1.4}$$

While in our numerical investigations we always use polynomial mappings, we expect the results to apply to a wider class of mappings (such as the polynomial-like mappings of Douady and Hubbard [28, 29]). When such mappings are used to model dynamical systems [24], with real variable z and real "non-linearity" parameter p, the asymptotic attractor can be conveniently represented by a "bifurcation tree," i.e., by a two-dimensional plot with p on one axis and values of the asymptotic iterates for given p plotted along the other axis [25, 7].

It is not possible to describe asymptotics of complex iterations in this way, as their iteration space has two (real) dimensions, and period n-tuplings are induced by adjusting a pair of (real) parameters.

In order to describe the properties of asymptotic iterates of complex mappings, we proceed in two steps.

First, we will describe the parameter dependence in terms of the associated Mandelbrot set M. The Mandelbrot set [26, 27] is the set of all values of the parameter of a quadratic mapping (parameter p in (1.3)) for which the iterates of the finite critical point do not escape to infinity. (A critical point z_c is a value of z for which the mapping $f(z)$ has vanishing derivative, $f'(z_c) = 0$. In (1.3) $z = 0$ and $z = \infty$

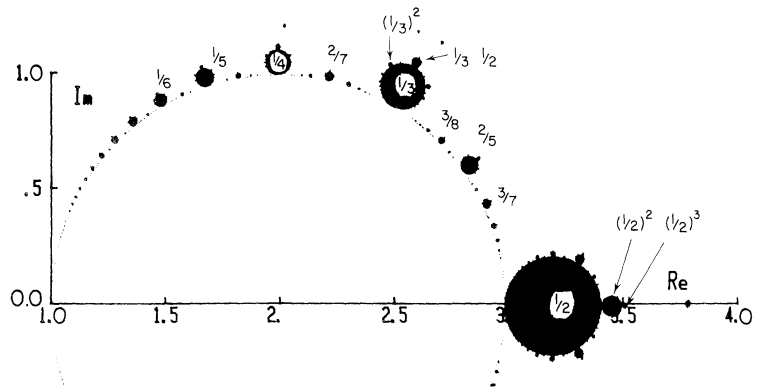

Fig. 1.1. The Mandelbrot set M is the region in the complex parameter plane for which the critical point of the mapping (1.4) does not iterate away to infinity. Inside the big circle (left open for clarity) iterations converge to a fixed point. The full region has two symmetry axes, $\mathrm{Re}\,\lambda = 1$ and $\mathrm{Im}\,\lambda = 0$, so only one quarter is shown. The usual period-doubling sequence is on the real axis. The winding numbers of the periodic orbits corresponding to larger leafs of M are indicated. See [27] for detailed scans of this region

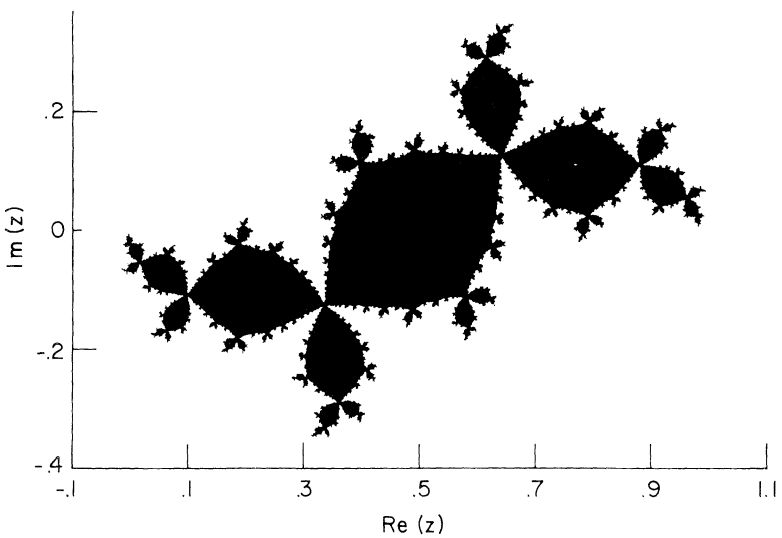

Fig. 1.2. The basin of attraction for the superstable 3-cycle of the Julia mapping (1.4). Any initial z from the black region converges toward the superstable 3-cycle, denoted by the three white dots. The basin of attraction for the Fatou mapping (1.3) superstable 3-cycle is the same, up to a coordinate shift and rescaling

are the critical points.) The Mandelbrot set for the mapping (1.4) is plotted in Fig. 1.1.

As explained below, what we actually use here is only the "Mandelbrot cactus," defined with respect to one particular critical point z_c, the associated fixed point and all of its bifuractions to attractive periodic orbits. The Mandelbrot cactus is well defined for general mappings (with higher order terms in (1.2)), even when the notion of "escape to infinity" is not meaningful.

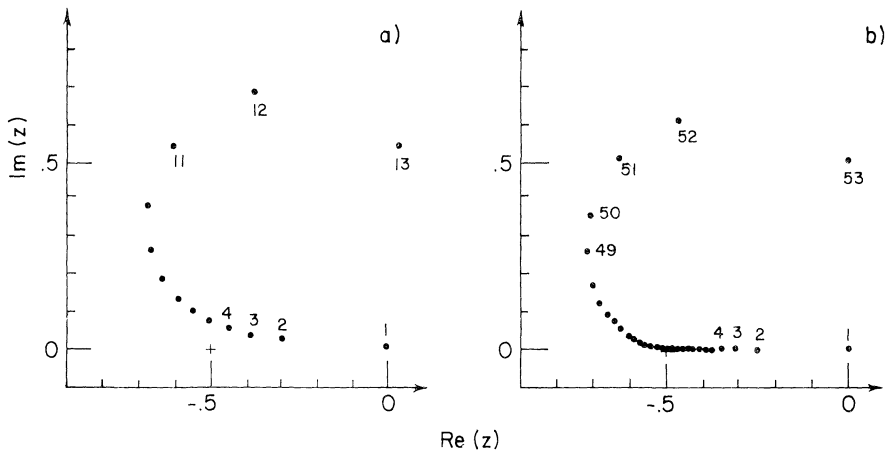

Fig. 1.3 (a) The attractor for the superstable 1/13-cycle of the Fatou mapping (1.3). (b) The attractor for the superstable 1/53-cycle. Any initial z from the basin of attraction converges asymptotically to the attractor.

Second, we describe the asymptotic iterates for a given value of the parameter by investigating either their attractor or their basin of attraction. In our applications the attractor L is always an attractive periodic orbit (cycle) z_0, $z_1, \ldots, z_{n-1}$. An orbit is periodic if the n^{th} iterate $z_n = f^n(z_0) = z_0$. If

$$\left|\frac{df^n(z_k)}{dz_k}\right| < 1\,, \tag{1.5}$$

the orbit is attractive. If the derivative (1.5) is vanishing, the orbit is superstable, and (by the chain rule) a critical point is one of the cycle points. For polynomial mappings $z = \infty$ plays a special role; it is always a superstable fixed point. A typical attractor is plotted in Fig. 1.3.

The general theory of iterations of analytic mappings is a rich and intricate subject. Here we investigate only periodic orbits associated with a given critical point (z_c in (1.2)). The following theorem due to Fatou [22] eases attractor searches:

Theorem. *The basin of attraction K of an attractive periodic orbit contains at least one critical point.*

The precise shape of the Mandelbrot set M depends on the particular mapping, but its core always resembles a self-similar cactus, see Fig. 1.1. The Mandelbrot cacuts is the set of connected components of M generated from a single fixed point attractor by all possible sequences of all possible period n-tuplings (see Sect. 3). The distinction between the Mandelbrot set and the Mandelbrot cactus is crucial; our arguments and our numerical evidence for universal scalings applies only to the cactuses. The Mandelbrot set is not self-similar; each level of magnification reveals more and more "hair."

The structure of the Mandelbrot set has been studied in detail by Douady and Hubbard [28, 29]. They have proven that M is connected, i.e., that the small Mandelbrot cactuses visible away from the main cactus in Fig. 1.1 are all

connected to the main cactus [30]. They have furthermore succeeded in characterizing Julia sets associated with various parts of M by unique combinatorial "trees" [31]. A particularly interesting Douady-Hubbard result is their determination of exterior angles associated with the boundary of M; for example, they have shown that the exterior angles associated with the period doubling sequence converge to the Thue-Morse number. The Thue-Morse number encodes the self-similar nature of period doublings in a direct way; it is defined by a self-similarity algorithm. This is the first analytic number in the universality theory for period n-tuplings; unfortunately, it is a measure of the exterior of the Mandelbrot set, and is unrelated to the physically interesting scaling of the interior, the Feigenbaum [1, 32] δ.

To summarize, the parameter dependence of asymptotic iterates of mapping $f(z)$ is described by the Mandelbrot set M. For each point inside the Mandelbrot cactus, the asymptotic iterates can be described by their basin of attraction K, the Julia set J and the attractor L.

2. Two-Dimensional Mappings

In this section we briefly discuss general two-dimensional mappings. This analysis is not new, but it is cast in a form suited to our purposes. Our conclusion will be that the analytic mappings are atypical and that we do not expect the universal properties of iterates of complex functions (developed in the remainder of this article) to be characteristic of general two-dimensional systems.

Consider a two-dimensional mapping,

$$x_i \to x_i' = f_i(x), \qquad i = 1, 2. \tag{2.1}$$

We shall be interested in the stability of the periodic orbits (cycles) of such mappings. The elements of a cycle of length n are fixed points of the n^{th} iterate of $f(x)$,

$$x_k = f^n(x_k), \qquad k = 0, 1, 2, \ldots, n-1, \tag{2.2}$$

(here we have suppressed the vector index i; the subscript k labels the k^{th} cycle point). In this way the problem of determining the stability of a periodic orbit reduces to the study of the stability of fixed points of $g(x) = f^n(x)$. Stability of a fixed point is determined by the eigenvalues of the Jacobi matrix (except when the eigenvalue or largest modulus is exactly on the unit circle)

$$A_{jk} = \frac{\partial f_j}{\partial x_k}. \tag{2.3}$$

The orbit is stable (attractive) if $|\lambda_j| < 1$, $j = 1, 2$. Since A is a real matrix, the eigenvalues λ_j are either real, or form a complex conjugate pair λ, λ^*.

A stable orbit becomes unstable when one or more eigenvalues cross the unit circle. If a single real eigenvalue dominates, the transition must occur at either $\lambda = 1$ or $\lambda = -1$. For $\lambda = -1$ the system undergoes a period-doubling bifurcation which can be understood in terms of a one-dimensional real mapping [7]. Here we shall be interested in the case of the pair of complex eigenvalues λ, λ^* crossing the unit circle simultaneously.

To bring a general two-dimensional real mapping to a standard form in the neighborhood of a fixed point, we first shift the origin to the fixed point, and then use the eigenvalues of the Jacobi matrix (2.3) to construct projection operators

$$P=(A-\lambda^*\mathbb{1})/(\lambda-\lambda^*), \quad P^*=(A-\lambda\mathbb{1})/(\lambda^*-\lambda)$$

onto the two eigenvectors u, u^*: $Px=zu$, $P^*x=z^*u^*$. Then the action of the linear part of the mapping (2.1), i.e., the Jacobi matrix A, is just multiplication of z by λ:

$$Ax=\lambda zu+\lambda^* z^* u^* .$$

In terms of the complex variable z the nonlinear mapping (2.1) is given by

$$z\to z'=\lambda z+a_{20}z^2+a_{11}zz^*+a_{02}z^{*2}+a_{30}z^3+a_{31}z^2z^*+\ldots . \tag{2.4}$$

A general two-dimensional mapping is non-analytic, i.e., it depends on both z and z^*.

The next step in turning the mapping into a standard form is a non-linear change of variables [33, 34]

$$z\to w=z+b_{20}z^2+b_{11}zz^*+b_{02}z^{*2}+b_{30}z^3+b_{31}z^2z^*+\ldots . \tag{2.5}$$

In terms of the new variable w the iteration is given by

$$\begin{aligned} w' &= \lambda w+\sum_{j+k\geq 2} c_{jk}w^j w^{*k}, \\ c_{jk} &= a_{jk}+b_{jk}(\lambda^j\lambda^{*k}-\lambda)+\text{“}\ldots\text{”}. \end{aligned} \tag{2.6}$$

In the last sum “...” represents terms containing b_{lm} with $l+m<j+k$. For increasing values of $j+k$ the coefficients b_{jk} can be chosen successively so as to make $c_{jk}=0$ in (2.6), except at the resonances

$$\lambda^{j-k-1}=1 . \tag{2.7}$$

If λ is close to a resonance, the resonant terms in (2.6) must be kept, as otherwise the change of variable from z to w is a singular function of the parameter λ.

To study the way in which a fixed point turns into a stable n-cycle, consider λ with value close to the n^{th} root of unity

$$\omega=\exp(i2\pi m/n). \tag{2.8}$$

For λ close to the resonance the leading resonant terms in (2.6) are (changing the notation back to z instead of w)

$$\begin{aligned} z'=\lambda z(1+c_1|z|^2+c_2|z|^4+\ldots)+Az^{*n-1}(1+d_1|z|^2+d_2|z|^4+\ldots) \\ +Bz^{n+1}(1+e_1|z|^2+e_2|z|^4+\ldots)+\ldots . \end{aligned} \tag{2.9}$$

Depending on the nature of leading terms, this mapping can exhibit various types of bifurcations. The mapping

$$z\to z'=\lambda z(1+C|z|^2), \tag{2.10}$$

which represents the leading terms in (2.9) for $n>4$, exhibits a Hopf bifurcation. The fixed point $z=0$, which is stable for $|\lambda|<1$, gives birth to a stable invariant circle for $\mathrm{Re}\,C<0$ and $|\lambda|>1$. If $\mathrm{Re}\,C>0$ and $|\lambda|<1$ there is an unstable invariant

circle, which is absorbed by the fixed point at $|\lambda|=1$, so that for $\mathrm{Re}\, C>0$ and $|\lambda|>1$ there is no stable region close to $z=0$.

The mapping

$$z \to z' = \lambda z + z^{*n-1} \tag{2.11}$$

represents the leading terms in (2.9) for $n=3$. It has an n-cycle $z_0, z_1, \ldots, z_n = z_0$ with

$$z_k = \omega^k z_0\,, \qquad z_k^n = (\omega^* - \lambda^*)\,|z_k|^2 \tag{2.12}$$

which coincides with the fixed point $z=0$ when $\lambda=\omega$ (λ is then the n^{th} root of unity, (2.8)). This n-cycle is always unstable, and there is an explosive transition as soon as the fixed point becomes unstable.

The analytic mapping (set $B=1$ in (2.9) by rescaling z)

$$z \to z' = \lambda z + z^{n+1} \tag{2.13}$$

represents the leading terms in (2.9) *only if* an extra symmetry of the mapping (2.1) makes the non-analytic terms in (2.9) vanish. The properties of analytic mappings that we shall develop here depend crucially on the analyticity assumption, and are thus atypical of general two-dimensional mappings. (See Sect. 7 for comments on non-analytic perturbations).

3. Period n-Tupling

In this section we study the way in which a fixed point of the complex mapping (1.1) branches into an n-cycle. As in (2.3), the stability of a fixed point is given by

$$\varrho = \frac{dz_n}{dz_0}, \tag{3.1}$$

and we take, without loss of generality, the fixed point to be at $z=0$, and $f(z)$ with a power series expansion

$$f(z) = \varrho z + \sum_{j \geqq 2} a_j z^j\,. \tag{3.2}$$

As in (2.5), we change the variable

$$w = z + \sum_{j \geqq 2} b_j z^j \tag{3.3}$$

and eliminate from (3.2) all terms with $\varrho^j - \varrho \neq 0$ by fixing successively $b_2, b_3, \ldots$. If ϱ is sufficiently close to an n^{th} root of unity, $\omega = \exp(i2\pi m/n)$, and z is close to 0, the generic behavior of the new iteration function is the same as

$$f(z) = \varrho z + z^{n+1}\,. \tag{3.4}$$

In our numerical studies we assume the generic situation. This function has an n-cycle

$$z_j = \omega^j z_0\,, \qquad z_0^n = \omega - \varrho\,. \tag{3.5}$$

For $\varrho=\omega$ this n-cycle coincides with the fixed point $z=0$. In the neighborhood of $\varrho=\omega$ we have

$$dz_n/dz_0 = f'(z_0)f'(z_1)\ldots f'(z_{n-1})$$
$$=(\varrho+(n+1)z_0^n)^n = 1-(\varrho-\omega)n^2/\omega+\ldots . \tag{3.6}$$

For $\varrho=(1+\varepsilon)\omega$ the n-cycle (3.5) of the mapping (3.4) is stable if

$$|1-n\varepsilon|<1 , \tag{3.7}$$

while the fixed point is stable if

$$|1+\varepsilon|<1 . \tag{3.8}$$

The normal form mapping (3.4) is equivalent to (3.2) only for small z, and we do not rely on this equivalence in our numerical studies. However, (3.4) provides a good qualitative illustration of how a fixed point of (3.2) becomes unstable and branches into n-cycle.

In conclusion, in a generic situation, whenever a fixed point becomes unstable at $\varrho=n^{\text{th}}$ root of unity, it branches into an n-cycle which immediately becomes stable. As any stable cycle becomes unstable in the same fashion, branching into a new stable cycle with a multiple of the original cycle length, and as any such cycle is stable inside a disklike region in the complex parameter plane, the union of all these stability regions is a self-similar *Mandelbrot cactus*, introduced in Sect. 1.

4. Universal Equations for Period n-Tuplings

We now start with the analysis of infinite sequences of period n-tuplings, and give evidence for their conjectured universality.

As discussed above, a stable n^k-cycle becomes unstable and branches into an n^{k+1}-cycle when the parameter λ passes through a value such that the stability $\varrho_k(\lambda)$ (as defined in (3.1)) attains the critical value

$$\varrho(\lambda)=\omega=\exp(i2\pi m/n) . \tag{4.1}$$

For ϱ sufficiently close to this value the system is modeled by (3.4). From (3.6) it follows that near the transition from an n^k-cycle to an n^{k+1}-cycle

$$\varrho_{k+1}=1-(\varrho_k-\omega)\frac{n^2}{\omega}+\ldots , \tag{4.2}$$

hence

$$\left.\frac{d\varrho_{k+1}}{d\lambda}\right|_{\varrho_{k+1}=1} = -\frac{n^2}{\omega}\left.\frac{d\varrho_k}{d\lambda}\right|_{p_k=\omega} , \tag{4.3}$$

and at the transition there is a scale change by the complex factor [35] $-n^2/\omega$ which is independent of k.

Each leaf of the Mandelbrot cactus Fig. 1.1 corresponds to an m/n cycle, and the parameter value for the superstable m/n cycle corresponds to the center of the leaf. The above argument suggests that the leaf is n^2 times smaller than the cactus, and that it is rotated by a phase factor $-1/\omega$. The very geometry of the Mandelbrot cactus Fig. 1.1 suggests such scaling [36]. This scaling is not exact,

because the above analysis applies only to the infinitesimal neighborhood of the junction of a leaf to the cactus; however, the evaluation of the exact scaling numbers shows that this is a rather good approximation.

The exact scaling is obtained by comparing values of the parameter λ corresponding to successive $(m/n)^k$ superstable cycles, i.e., λ values such that $\varrho_k(\lambda_k)=0$. As each cactus leaf is similar to the entire cactus, we expect the ratios of the sizes of the successive stability regions corresponding to successive $(m/n)^k$-cycles to tend to a limit as $k\to\infty$:

$$\delta_{m/n}=\lim_{k\to\infty}\frac{\lambda_k-\lambda_{k-1}}{\lambda_{k+1}-\lambda_k}. \tag{4.4}$$

The scaling number δ tells us by how much we have to change the parameter λ in order to cause the next m/n period n-tupling. In particular, $\delta_{1/2}=4.669\ldots$ is the Feigenbaum δ for the period doublings in real one-dimensional mappings [1, 32].

An alternative definition of δ is

$$\delta_{m/n}=\lim_{k\to\infty}\frac{\left.\frac{d\varrho_{k+1}}{d\lambda}\right|_{\varrho_{k+1}=c}}{\left.\frac{d\varrho_k}{d\lambda}\right|_{\varrho_k=c}}. \tag{4.5}$$

Here we compare the scales of successive stability regions at given stability ϱ. For $\varrho=1$ Eq. (4.3) yields the approximation

$$\delta_{m/n}\cong-\frac{n^2}{\omega}=n^2 e^{-i2\pi(m/n-1/2)}. \tag{4.6}$$

We conclude that $\delta_{m/n}\to-n^2/\omega$ as $m/n\to 0$, exactly. This conjecture is supported by the numerical evaluation of δ's, Sect. 6.

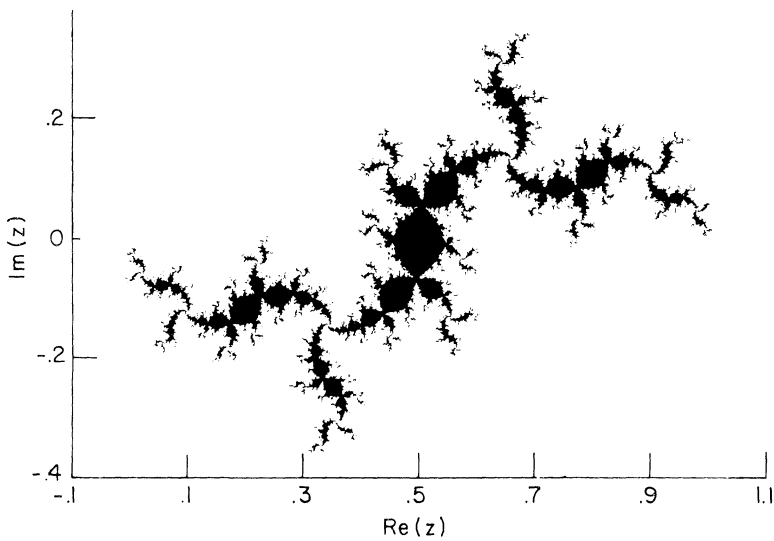

Fig. 4.1. The basin of attraction for the superstable 9-cycle for iterates of the model mapping (1.4). The scaled down version of the 3-cycle basin of attraction, Fig. 1.2, is visible in the center

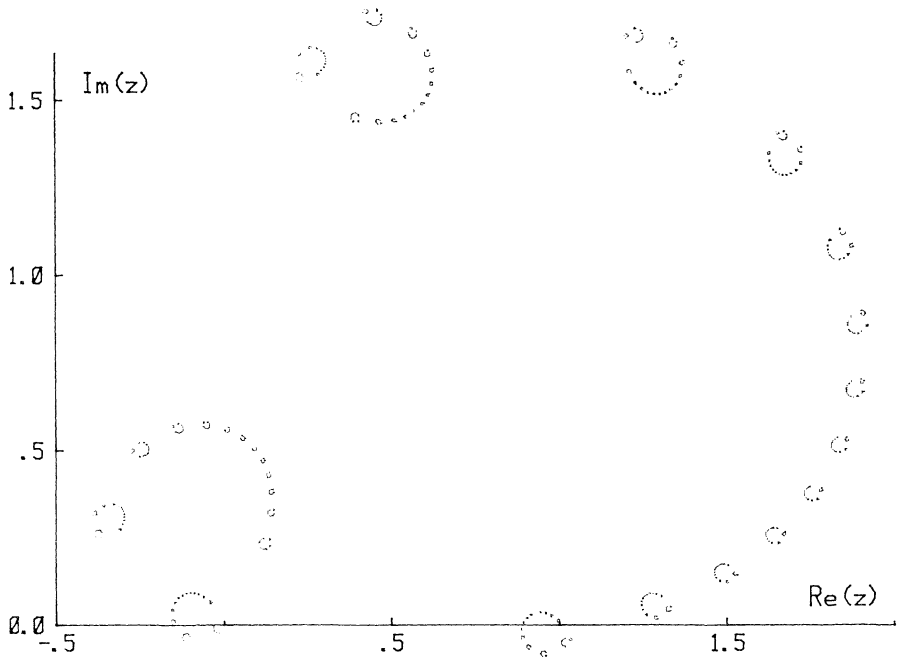

Fig. 4.2. The first 30,000 points of the attractor for $1/13^{\infty}$-cycle, or the "universal 1/13 horseshoe." The smaller horseshoe at the origin is identical to the full horseshoe, except for a scaling and rotation by the complex scaling factor $\alpha_{1/13}$

Scaling in the parameter space (generalized Feigenbaum's δ) is suggested by the apparent self-similarity of the Mandelbrot cactuses [37]. In the same way the self-similarity of the Jula sets (or the asymptotic attractors) suggests a scaling law in the iteration space z, which we discuss next. This law will characterize the scales of successive trajectory splittings (generalized Feigenbaum's α).

The self-similarity we are alluding to can be seen by comparing the basin of attraction for the superstable 3-cycle, Fig. 1.2, and for the superstable 9-cycle, Fig. 4.1. In the latter figure the 3-cycle basin of attraction is visible in the center, rotated and scaled down by a factor whose asymptotic limit is the generalization of Feigenbaum's α to period triplings.

This scaling number α can be computed by comparing the successive superstable cycles, at successive parameter values λ_k, λ_{k+1}. As $k\to\infty$, the sequence of λ_k's converges to λ_∞, and the superstable n^k-cycles converge to an n^∞-cycle which looks typically like a series of nested horseshoes, Fig. 4.2.

In Fig. 4.2 the sequence $z_0\to z_1\to z_2\to\ldots\to z_{12}$ traces out a large horeseshoe. The sequence $z_0\to z_{13}\to z_{26}\to\ldots\to z_{156}$ traces out a smaller horseshoe, and so forth. The attractor is self-similar: the horseshoes on succeeding levels are related by rescaling and rotation by a complex number which asymptotically approaches

$$\alpha_{m/n}=\lim_{k\to\infty}\frac{z_n^k-z_0}{z_n^{k+1}-z_0}. \tag{4.7}$$

α characterizes the scale of trajectory splitting at each period n-tupling. (For $m/n=1/2$ this is Feigenbaum's [1] $\alpha=-2.5029\ldots$.)

We do not have as good an intuitive picture for estimating α's as we have for δ's. Very roughly, the size of α is inversely proportional to the gap of the "horseshoe," as the successive horseshoes have to be fitted within each other. For $1/n$-tuplings the size of the gap is insensitive to n, as the two cycle points which define the gap, the critical point and its first preimage, depend weakly on n. For this reason the 1/53 cycle, Fig. 1.3b, does not look very different from the 1/13 cycle, Fig. 1.3a, and the corresponding α's converge to finite limits in the $n\to\infty$ limit.

We can use the results of Sect. 3 to argue that $\alpha_{1/n}$ approaches a finite limit as $n\to\infty$, and that the convergence is logarithmic. Close to the period n-tupling parameter value $\varrho=\omega$ in (3.4), the cycle points (3.5) are uniformly spaced with angle $2\pi/n$ at radius $|\varrho-\omega|^{1/n}$. Close to the period n-tupling parameter value p_1 the cycle points of the original mapping (consider for concreteness the Fatou mapping (1.3)) behave similarly. As the parameter value in (1.3) is smoothly changed from p_1 to the superstable n-cycle value p_s, the cycle fans out. Let $z_0(p)$ be that periodic point which eventually falls onto the critical point, $z_0(p_s)=z_c$. For the superstable cycle the distances between the critical point, its image and its preimage are of order 1, and (because the critical point is quadratic) the three cycle points subtend an angle of $\pi/2$ (see Fig. 1.3). Consider next the parameter value p_2 corresponding to the period n-tupling of the n-cycle. Then

$$\alpha_{1/n}\propto\frac{z_0(p_1)-z_c}{z_0(p_2)-z_c}.$$

In what follows we assume that the transformation (3.3) is valid up to the critical point z_c, in order to be able to estimate $z_0(p_2)$ from the model mapping (3.4). The corresponding parameter value ϱ_2 in the model mapping (3.4) is determined by setting the derivative (3.6) equal to ω. This yields a cycle point $z_0(\varrho_2)$ located between the superstable cycle point $z_0(\varrho_s)$ and the fixed point $z_0(\omega)$. In the model mapping the critical point, its image and its preimage subtend an angle of nearly π, and $z_0(\varrho_2)$ lies at an angle of approximately $\pi/2$ with respect to z_c and its image. If the original mapping has a quadratic critical point, the angles at the critical point are approximately halved by the inverse of transformation (3.3). On the basis of above arguments we expect that: the phase of $a_{1/n}$ in (4.8) is approximately $\pi/4$, that $|a_{1/n}|$ approaches a non-zero constant (as the exact location of $z_0(\varrho_2)$ depends on the mapping, a simple analytic expression for the limit of $a_{1/n}$ is unlikely), and that the convergence should be logarithmic, $a_{1/n}-a_{1/\infty}=O(1/n)$. We have checked this numerically for n up to 50, and find $|a_{1/(n+1)}-a_{1/n}|\propto n^{-2.01\cdots}$. The above arguments can be straightforwardly generalized to other families of period n-tuplings (such as those discussed in Sect. 7).

For m/n-cycles with $m>1$ the horseshoe gap is smaller, because some of the cycle points fall between the critical point and its preimage, and correspondingly the α's are larger. The extreme case obtains for m/n's approximants to irrational numbers. In Fig. 4.3 we have plotted the attractor for the superstable 987/1597 cycle. 987/1597 is an approximation to the golden mean, and the attractor does not resemble a horseshoe at all: as for $m/n\to(\sqrt{5}-1)/2$ the cycle points become dense [34], the gap at the critical point is very small, and correspondingly the α is very large.

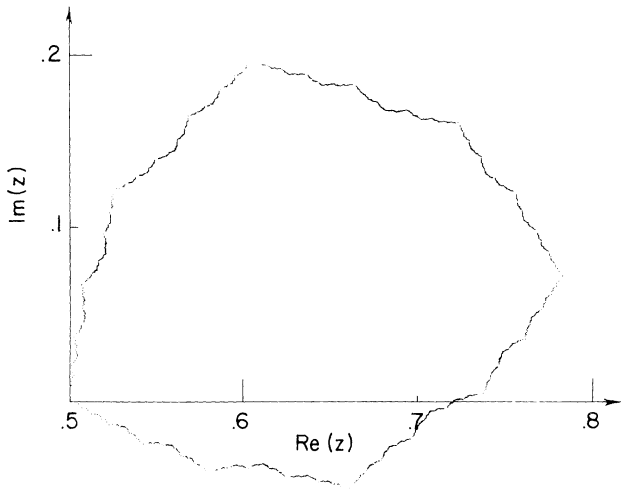

Fig. 4.3. The attractor for the superstable 987/1597 cycle for mapping (1.3). 987/1597 is an approximation to the golden mean. In the limit $m/n \to (\sqrt{5}-1)/2$ the cycle points fill out the trajectory densely

Denote by T the operation of iterating n-times (in the above example $n=13$) and rescaling by α:

$$Tf(z) = \alpha f^n(z/\alpha). \tag{4.8}$$

The operation T encodes the self-similarity of the asymptotic cycle; it maps each horseshoe into a horseshoe on the preceding level.

After iterating and magnifying the neighborhood of the critical point by T infinitely many times, all information about the global shape of the starting function $f(z)$ is lost, and we expect to be left with a universal function $g(z) = g_{m/n}(z)$ which is self-reproducing under rescaling and iteration:

$$g(z) = \alpha g^n(z/\alpha). \tag{4.9}$$

This university equation describes the asymptotics of infinite sequences of (m/n) period n-tuplings. It determines the universal scaling numbers α and δ; we shall solve it numerically in Sect. 6. The universality equation for period doubling [38] is the special, $n=2$, case of this equation.

Similar universality equations can be defined for other itineraries of period n-tuplings. (We have not pursued this further, other than with a cursory investigation of the $1/3 \to 2/3 \to 1/3 \to 2/3 \to \ldots$ sequence.)

5. Unstable Manifold

In this section we describe the elegant formulation of the universality theory due to Vul et al. [39, 3, 40, 41].

The universality equation (4.9) encodes the self-similarity of the asymptotic superstable orbit. However, the self-similarity extends to the parameter space as

well: not only does the asymptotic orbit resemble itself under rescaling and rotation by α, but also each leaf of the Mandelbrot cactus resembles the entire cactus under rescaling and rotation by δ.

These self-similarities can be described by means of the following three operations:

The first operation is a rescaling of the parameter and iteration spaces:

$$[Rf]_p(z) = af_{p/d}(z/a). \tag{5.1}$$

With the appropriate choice of complex numbers d (a), a leaf of the Mandelbrot cactus (a horseshoe within the attractor) can be rescaled and rotated to the size and the orientation of the entire cacuts (entire attractor).

We fix the origin of p and z by requiring that $z=0$ be a critical point of the mapping $f_p(z)$, and, for the parameter value $p=0$, a superstable fixed point as well (the Fatou mapping (1.3) is an example of such a mapping). We fix the scale of p and z by requiring that the superstable m/n cycle occurs for the parameter value $p=1$ and that

$$f_1(0) = 1. \tag{5.2}$$

The second operation shifts the origin of the parameter space to the center of the m/n-leaf of the Mandelbrot cactus (p corresponding to the superstable m/n cycle):

$$[Sf]_p(z) = f_{1+p}(z). \tag{5.3}$$

The third operation iterates $f_p(z)$ n times:

$$[Nf]_p(z) = f_p^n(z). \tag{5.4}$$

By definition, $[Sf]_0(z) = f_1(z)$ has a superstable m/n cycle, so its n^{th} iterate has a superstable fixed point, $[NSf]_0(0) = 0$.

The parameter shift S overlays the Mandelbrot cactus over its m/n leaf, and the Julia set for $[Nf]_1(z)$ resembles the Julia set for the superstable fixed point $f_0(z)$ (see Fig. 1.2 and Fig. 1.4, for example). Finally we adjust the scale of the new M, J sets by requiring that the scale factors a, d in (5.1) are such that $[RNSf]_p(z)$ satisfies the same normalization condition (5.2) as the initial function $f_p(z)$. This shifting and rescaling is illustrated in Fig. 5.1.

The combined effect of the rescaling, parameter shift and iteration is summarized by the operator $T^* = RNS$;

$$[T^*f]_p(z) = af_{1+p/d}^n(z/a). \tag{5.5}$$

If we take a polynomial $f_p(z)$ and act on it with T^*, the result will be a polynomial of higher degree with similar M and J sets. For a finite number of T^* operations the scaling numbers d and a depend on the choice of the initial mapping $f_p(z)$. If we apply T^* infinitely many times, we expect that a and d will converge to the universal limits a and δ, and $T^{*n}f_p(z)$ will converge to a universal one-parameter family which is a fixed point of the operator T^*:

$$g_p(z) = [T^*g]_p(z) = \alpha g_{1+p/\delta}^n(z/\alpha). \tag{5.6}$$

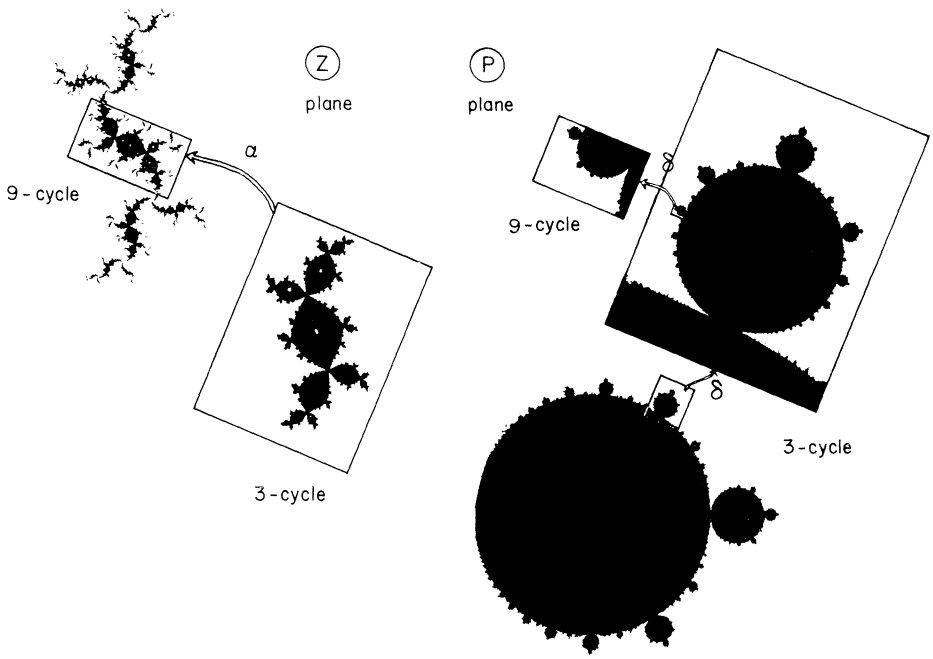

Fig. 5.1. The unstable manifold method illustrated by period triplings. The parameter is shifted from the center of a cactus leaf to its 1/3 leaf, the 1/3 leaf is rescaled and rotated by δ, and the basin of attraction of third iterates is rescaled and rotated by α. The Mandelbrot cactus and the basin of attraction for the unstable manifold g_p are self-similar under such shifting and rescaling

This universality equation determines both $g_p(z)$ and the universal numbers α and δ. Our original universality equation (4.9) is a special case of the above equation: $g(z)=g_{p^*}(z)$, where

$$p^*=1+p^*/\delta\,. \tag{5.7}$$

p^* is the parameter value corresponding to the asymptotic $(m/n)^\infty$-cycle. The family of universal functions $g_p(z)$ is called the unstable manifold because it is invariant under the T-operation (4.8) which drives p away from the fixed point value p^*:

$$[Tg]_p(z)=\alpha g_{p^*+\delta(p-p^*)}(z/\alpha)\,. \tag{5.8}$$

To summarize, the T^* operation encodes simultaneously the self-similarity in the parameter space (Mandelbrot cactuses) and in the iteration space (Julia sets). Being no more than a redefinition of variables, it is exact, and it is an explicit implementation of the above self-similarities; T^* magnifies the nth iterate of the $(m/n)^{k+1}$-cycle and overlays it onto the $(m/n)^k$-cycle (see Fig. 5.1). Asymptotically we expect that the self-similarity will become exact, and hence that the procedure will converge to the unstable manifold, a one dimensional line of universal functions g_p.

Not only are the N, S, R operations *a* natural encoding of the complex universality, but, as we shall see in the next section, they are also useful computational tools.

6. Numerical Solutions of Universality Equations

In the neighborhood of the critical point $z=0$, the universal function $g(z)$ is basically a parabola, and is well approximated by a truncated power series. This observation leads to a simple and efficient method [42] for solving (4.9). Approximate $g(z)$ by an $2n^{\text{th}}$ order polynomial,

$$g(z)=1+\sum_{j\geq 1} a_j z^{2j}. \tag{6.1}$$

The universal equation (4.9) determines $g(z)$ up to an overall scale, which we fix by the normalization condition

$$g(0)=1. \tag{6.2}$$

The renormalization operator T from (4.8) maps (6.1) into a new polynomial, which we also truncate to the order $2N$:

$$[Tg](z)=1+\sum_{j\geq 1} b_j z^{2j}. \tag{6.3}$$

With this truncation, the universality equation (4.9) reduces to a set of N equations obtained by equating the coefficients in (6.1) and (6.3). These equations can be solved by the standard Newton-Raphson method, provided one starts with a sufficiently good guess. The Newton-Raphson method requires inversion of the $N\times N$ jacobian matrix

$$D_{jk}=\frac{\partial b_j}{\partial a_k}. \tag{6.4}$$

We choose a_1 in the starting approximation $g(z)=1+a_1 z^2$ corresponding to the $(m/n)^\infty$ cycle (an extrapolation from the m/n and $(m/n)^2$ cycle is sufficient), and carry out the first few iterations without Newton-Raphson correction. As in the period-doubling case [2], iteration without Newton-Raphson correction would eventually diverge, because D_{jk} has a single unstable eigenvalue, namely δ. (Needless to say, in each calculation we have verified that there is only one unstable eigenvalue, and no marginal eigenvalues.)

When the solution for $a_1, a_2, \ldots, a_N$ of the desired accuracy is found, α follows from the normalization (6.2) and the universal equation (4.9),

$$1/\alpha=g^n(0), \tag{6.5}$$

and $\delta=\delta_{m/n}$ is the single eigenvalue of the jacobian matrix D with norm greater than 1.

The α's and δ's computed this way are listed in Table 6.1. The universal function coefficients for $m/n=1/3$ and $1/63$ are listed in Tables 6.2 and 6.3. Typically a 12 term approximation to $g(z)$ for a short cycle (n small), with 17 significant digits precision, yields α to 8 significant digits and δ to 6 significant digits. For long cycles, such as $n=60$, the precision goes down and a 15 term approximation is needed to obtain 4 significant digits for α and 2 significants digits for δ.

The unstable manifold universal equation (5.6) provides an alternative method for computing the scaling numbers α and δ.

Table 6.1. Universal numbers α and δ

m/n	Re(α)	Im(α)	Re(δ)	Im(δ)
1/2	− 2.5029079		4.669202	
1/3	− 2.0969199	2.3583	4.600225	8.981226
1/4	− 1.1315	3.2600	− 0.8527	18.1097
1/5	− 0.3800	3.5539	− 9.520	26.371
1/6	0.1600	3.6264	− 20.657	34.009
1/7	0.5524	3.6152	− 33.991	41.238
1/8	0.8455	3.5724	− 49.413	48.195
1/9	1.0704	3.5191	− 66.875	54.965
1/10	1.2474	3.4641	− 86.35	61.60
1/11	1.3898	3.4113	− 107.84	68.14
1/12	1.5065	3.3619	− 131.33	74.61
1/13	1.6036	3.3165	− 156.82	81.02
1/14	1.6856	3.2750	− 184.30	87.38
1/15	1.7556	3.2371	− 231.79	93.71
1/17	1.8688	3.1709	− 278.74	106.29
1/19	1.9561	3.1154	− 351.69	118.78
1/20	1.9926	3.0910	− 391.16	125.01
1/22	2.0549	3.0477	− 476.1	137.4
1/23	2.0816	3.0284	− 521.5	143.6
1/25	2.1282	2.9938	− 618.5	156.0
1/27	2.1673	2.9638	− 723.4	168.3
1/29	2.2006	2.9374	− 836.3	180.7
1/33	2.254	2.893	−1086.0	205.0
1/38	2.305	2.850	−1443.0	236.0
1/43	2.342	2.817	−1851.0	267.0
1/48	2.372	2.790	−2309.0	297.0
1/53	2.396	2.767	−2817.0	328.0
1/58	2.415	2.749	−3376.0	359.0
1/63	2.431	2.733	−3979.0	389.0
2/5	− 3.8741	2.1810	18.969	14.564
2/7	− 2.3939	4.3486	6.681	47.499
2/9	− 1.0781	5.0877	− 20.805	78.221
2/11	− 0.1323	5.3170	− 59.07	106.71
2/13	0.5452	5.3563	− 106.55	133.68
2/15	1.0438	5.3219	− 162.62	159.63
2/17	1.4219	5.2597	− 227.01	184.88
2/19	1.7166	5.1889	− 299.57	209.65
2/21	1.9516	5.1179	− 380.2	234.1
2/23	2.1429	5.0500	− 469.0	258.2
2/25	2.3013	4.9868	− 565.7	282.1
2/27	2.4343	4.9285	− 670.5	305.6
2/29	2.5476	4.8750	− 783.3	329.6
2/31	2.645	4.826	− 904.0	353.0
2/33	2.730	4.781	−1033.0	377.0
2/35	2.804	4.740	−1170.0	400.0
2/37	2.870	4.702	−1315.0	423.0
2/39	2.928	4.667	−1468.0	447.0
2/41	2.980	4.635	−1628.0	470.0
2/43	3.027	4.606	−1797.0	493.0
3/7	− 4.9851	2.1097	39.855	17.345

Table 6.1 (continued)

m/n	Re(α)	Im(α)	Re(δ)	Im(δ)
3/8	− 4.7509	3.3158	37.150	45.836
3/10	− 3.1205	5.2781	21.89	87.04
3/11	− 2.9301	5.6292	2.31	116.75
3/13	− 1.3347	6.3452	− 32.62	154.24
3/14	− 1.3985	6.4515	− 63.87	182.82
3/16	− 0.0541	6.6681	− 112.40	217.03
3/17	− 0.2925	6.7284	− 153.42	244.60
3/19	0.8552	6.7201	− 213.42	276.63
3/20	0.5086	6.7931	− 263.44	303.47
3/22	1.5190	6.6697	− 334.1	334.0
3/23	1.1046	6.7710	− 392.7	360.4
3/25	2.0187	6.5817	− 473.6	390.0
3/26	1.5608	6.7135	− 540.7	415.9
3/28	2.4058	6.4828	− 631.6	444.8
3/29	1.9193	6.6430	− 707.0	470.4
4/9	− 5.7943	2.1951	67.747	17.723
4/11	− 5.6058	3.9917	60.43	94.38
4/13	− 3.5324	6.1283	46.11	137.06
4/15	− 3.5989	6.5440	− 7.86	218.56
4/17	− 1.3190	7.4041	− 42.98	255.14
4/19	− 1.9110	7.5014	− 129.84	334.39
4/21	− 0.2510	7.7562	− 178.2	366.2
4/23	− 0.6788	7.8563	− 292.7	443.1
4/25	1.3540	7.7832	− 351.7	471.9
4/27	0.2228	7.9672	− 491.8	547.0
4/29	2.1518	7.6931	− 560.5	573.8
5/11	− 6.4041	2.3777	102.98	15.93
5/12	− 6.7255	3.1835	100.29	67.29
5/13	− 6.3563	4.3160	99.38	99.70
5/14	− 6.4061	4.3805	89.49	160.62
5/16	− 3.7311	6.8847	80.08	198.07
5/17	− 4.3223	7.2268	38.55	256.40
5/18	− 3.7979	7.6067	16.39	287.29
5/19	− 4.3015	7.1836	− 23.16	353.86
5/21	− 1.1342	8.2725	− 50.9	381.8
5/22	− 2.0294	8.6464	− 120.1	437.7
5/23	− 1.6364	8.7522	− 155.2	465.4
5/24	− 2.5054	8.2873	− 218.1	534.3
5/26	0.6810	8.6054	− 255.3	555.6
5/27	− 0.3642	9.1168	− 347.6	607.8
5/28	− 0.0835	9.1221	− 392.9	633.1
5/29	− 1.1789	8.7300	− 476.4	704.0
6/13	− 6.8651	2.6080	145.73	12.13
6/17	− 7.1224	4.5767	124.81	244.72
6/19	− 3.7872	7.5373	124.14	270.55
6/23	− 4.9787	7.6141	− 43.0	523.1
6/25	− 0.8558	8.9662	− 56.1	535.1
6/29	− 3.1121	8.8593	− 327.9	783.1
7/15	− 7.2131	2.8540	196.09	6.44
7/16	− 8.0945	3.3267	187.88	84.51

Table 6.1 (continued)

m/n	Re(α)	Im(α)	Re(δ)	Im(δ)
7/17	− 8.3289	3.7122	190.21	154.27
7/18	− 7.4681	5.3939	197.42	168.70
7/19	− 7.7033	5.5577	178.29	241.27
7/20	− 7.7453	4.6456	166.72	346.69
7/22	− 3.7526	8.0885	178.4	354.9
7/23	− 5.0979	8.7039	100.7	445.5
7/24	− 5.6717	8.5847	57.3	525.3
7/25	− 4.1468	9.3493	51.7	528.9
7/26	− 4.7947	9.2319	− 10.2	604.6
7/27	− 5.6008	7.8909	− 67.0	726.4
7/29	− 0.5363	9.5106	− 58.4	715.6
8/17	− 7.4756	3.0970	254.11	− 1.03
8/19	− 8.6799	4.3522	248.37	139.33
8/21	− 8.6157	5.5690	235.4	282.8
8/23	− 8.2780	4.6329	215.4	466.5
8/25	− 3.6639	8.5484	242.9	451.3
8/27	− 5.2800	9.7055	110.6	606.2
8/29	− 5.4753	9.9420	9.0	759.0
9/19	− 7.6737	3.3275	319.80	− 10.23
9/20	− 9.1002	3.6413	300.39	97.89
9/22	− 9.7430	3.8618	312.5	279.5
9/23	− 8.2064	6.4631	334.8	253.6
9/25	− 8.9878	6.2691	277.8	443.3
9/26	− 8.7299	4.5697	271.1	604.1
9/28	− 3.5455	8.9305	317.5	560.0
9/29	− 5.4627	10.0265	189.9	684.3
10/21	− 7.8234	3.5413	393.2	− 21.1
10/23	−10.1954	3.8270	375.0	211.5
10/27	− 9.1320	7.1758	375.7	442.4
10/29	− 9.1123	4.4770	333.8	759.4
11/23	− 7.9367	3.7369	474.2	− 33.7
11/25	−10.3086	4.6906	452.5	169.6
11/26	−10.0829	5.6315	474.9	227.3
11/29	−10.7052	6.1850	436.1	573.5
11/30	−10.4267	6.8875	415.2	633.5
11/32	− 9.436	4.368	404.0	932.0
11/34	− 3.276	9.512	497.0	815.0
12/29	−11.3109	5.3929	539.4	376.9
12/31	−10.629	7.374	530.0	560.0
13/29	−11.5666	4.1977	614.9	266.9
13/31	−11.909	5.552	625.0	434.0
13/34	−11.169	7.841	622.0	661.0
14/29	− 8.1366	4.2218	763.5	− 81.0
14/41	−10.148	4.019	656.0	1557.0
14/43	− 2.885	10.077	842.0	1290.0
15/31	− 8.173	4.354	875.0	− 100.0
17/35	− 8.221	4.583	1122.0	− 143.0
21/43	− 8.256	4.931	1707.0	− 247.0
21/55	−15.539	9.920	1553.0	1883.0

Table 6.2. Universal function for period triplings $g_{1/3}(z)$. The first 9 coefficients in 11-term expansion (6.1). $E-4$ stands for $\times 10^{-4}$, etc.

k	$\mathrm{Re}(c_k)$	$\mathrm{Im}(c_k)$
0	1.0	0.0
1	0.54665 $E-1$	0.749021
2	−0.24397 $E-1$	0.52466 $E-1$
3	−0.2529 $E-2$	0.1197 $E-2$
4	−0.8808 $E-4$	−0.1376 $E-3$
5	0.7284 $E-6$	−0.1829 $E-4$
6	0.5413 $E-6$	−0.1193 $E-5$
7	0.7364 $E-7$	−0.4772 $E-7$
8	0.7354 $E-8$	0.2570 $E-9$
9	0.5806 $E-9$	0.2832 $E-9$

Table 6.3. Universal function $g_{1/63}(z)$. The first 11 coefficients in 14-term expansion (6.1)

k	$\mathrm{Re}(c_k)$	$\mathrm{Im}(c_k)$
0	1.0	0.0
1	0.316969	0.8639 $E-2$
2	−0.16147 $E-1$	−0.2718 $E-3$
3	−0.98843 $E-3$	−0.1264 $E-3$
4	−0.53994 $E-4$	0.2177 $E-4$
5	0.24356 $E-5$	−0.2049 $E-5$
6	−0.83356 $E-7$	0.1380 $E-6$
7	0.18778 $E-8$	−0.7286 $E-8$
8	−0.25073 $E-10$	0.3294 $E-9$
9	0.13966 $E-11$	−0.1556 $E-10$
10	−0.12662 $E-12$	0.9537 $E-12$
11	−0.11355 $E-14$	−0.6775 $E-13$

The universality equation (5.6) can be solved numerically by approximating [39, 3] the unstable manifold by a truncation of the double power series expansion for $g_p(z)$:

$$g_p = \sum_{j,k \geq 0}^{N} c_{jk} z^{2j} p^k . \tag{6.6}$$

We start with a two term approximation to $g_p(z)$: $g_p(z) = c_{01} p + c_{10} z^2$. Repeated applications of the T^* operation (5.5) generate a double polynomial in z and p of higher and higher degree; this procedure converges asymptotically to the unstable manifold $g_p(z)$. We implement the shifting and iteration operations S and N as numerical polynomial substitution routines, truncating all polynomials as in (6.6). The T^* operation is completed by the rescaling operation R, Eq. (5.1). The scaling numbers d and a are fixed by the normalization conditions (5.2). We use Newton's method to find the parameter value corresponding to the superstable m/n-cycle.

Table 6.4. Universal manifold $g_p(z)$ for period doublings, $m/n=1/2$. The coefficients in the expansion (6.6) for $j<9$, $k<10$ truncation

j \ i	0	1	2	3	4	5
0	0.0	−0.793586	0.55650 $E-1$	0.2472 $E-2$	−0.2615 $E-3$	0.821 $E-5$
1	0.747235	−0.253027	−0.3970 $E-2$	0.1845 $E-2$	−0.1013 $E-3$	0.462 $E-6$
2	0.239114	−0.93379 $E-2$	−0.4485 $E-2$	0.4430 $E-3$	−0.1193 $E-4$	−0.150 $E-5$
3	0.15297 $E-1$	0.4350 $E-2$	−0.8995 $E-3$	0.5241 $E-4$	0.2924 $E-5$	−0.596 $E-6$
4	−0.1294 $E-2$	0.8644 $E-3$	−0.1016 $E-3$	−0.1504 $E-5$	0.1395 $E-5$	−0.811 $E-7$
5	−0.3162 $E-3$	0.9378 $E-4$	−0.3187 $E-5$	−0.1888 $E-5$	0.2159 $E-6$	0.558 $E-8$
6	−0.3366 $E-4$	0.5115 $E-5$	0.1399 $E-5$	−0.3310 $E-6$	0.3577 $E-8$	0.397 $E-8$

Table 6.5. Universal manifold $g_p(z)$ for period triplings, $m/n=1/3$. The coefficients in the expansion (6.6), same truncation as Table 6.4. The first number is the real part, and the number below it is the imaginary part of c_{jk}

j \ i	0	1	2	3	4	5
0	0.0	−0.777638	0.88152 $E-1$	−0.5223 $E-2$	−0.1323 $E-3$	0.129 $E-4$
	0.0	−0.8161 $E-2$	0.6495 $E-2$	−0.8522 $E-3$	−0.2932 $E-3$	0.772 $E-4$
1	0.776422	−0.289828	0.24759 $E-1$	0.3096 $E-3$	−0.1740 $E-3$	0.659 $E-5$
	0.18070 $E-1$	−0.5851 $E-2$	−0.1244 $E-2$	0.1610 $E-2$	−0.5237 $E-3$	0.618 $E-4$
2	0.203142	−0.40248 $E-1$	0.7133 $E-4$	0.6615 $E-3$	−0.6834 $E-4$	0.111 $E-4$
	−0.8789 $E-2$	0.7453 $E-2$	−0.3987 $E-2$	0.1377 $E-2$	−0.2247 $E-3$	0.191 $E-4$
3	0.20459 $E-1$	−0.5605 $E-3$	−0.1097 $E-2$	0.2153 $E-3$	−0.3667 $E-4$	0.102 $E-4$
	−0.7044 $E-2$	0.4463 $E-2$	−0.1817 $E-2$	0.4124 $E-3$	−0.4695 $E-4$	0.363 $E-5$
4	0.3147 $E-3$	0.8668 $E-3$	−0.3132 $E-3$	0.6823 $E-4$	−0.1925 $E-4$	0.512 $E-5$
	−0.1869 $E-2$	0.1212 $E-2$	−0.4040 $E-3$	0.6462 $E-4$	−0.5207 $E-5$	0.693 $E-6$
5	−0.2695 $E-3$	0.2186 $E-3$	−0.7201 $E-4$	0.2317 $E-4$	−0.7293 $E-5$	0.172 $E-5$
	−0.3255 $E-3$	0.2002 $E-3$	−0.4906 $E-4$	0.4072 $E-5$	−0.1336 $E-7$	0.942 $E-7$
6	−0.5959 $E-4$	0.4007 $E-4$	−0.1733 $E-4$	0.6803 $E-5$	−0.2038 $E-5$	0.435 $E-6$
	−0.3891 $E-4$	0.1837 $E-4$	−0.1185 $E-5$	−0.8909 $E-6$	0.2372 $E-6$	−0.520 $E-7$

This determines d, and a then follows directly from the condition (5.2). The result is a new approximation to $g_p(z)$. Asymptotically d's converge to δ and a's converge to α. We keep applying the truncated T^* operation until the coefficients in (6.6) repeat.

The coefficients c_{jk} for $m/n=1/2$ and $1/3$ unstable manifolds, given in Tables 6.4 and 6.5, are typical of our results. Here we have normalized g_p by the superstable 2-cycle,

$$g_0(0)=0\,, \quad g_1(0)=1\,, \quad g_1(1)=0\,. \tag{6.7}$$

In our calculations we actually use the superstable m/n-cycle normalization (5.2), but the 2-cycle normalization convention is more convenient for comparing different m/n unstable manifolds: it aligns the universal Mandelbrot cactuses (see the next paragraph) for different m/n sequences the same way.

In the period-doubling case the (real) universal function $g(x)$ is easily plotted as a function of the real variable x. In the complex case, there is no natural way to plot the universal functions; the best we can do is to represent the unstable manifold $g_p(z)$ by the associated Mandelbrot and Julia sets. As the universality equations are based on the self-similarity of Mandelbrot cactuses, the "universal Mandelbrot" cactuses (see Fig. 6.1 and Fig. 6.2) do not look very different from the starting

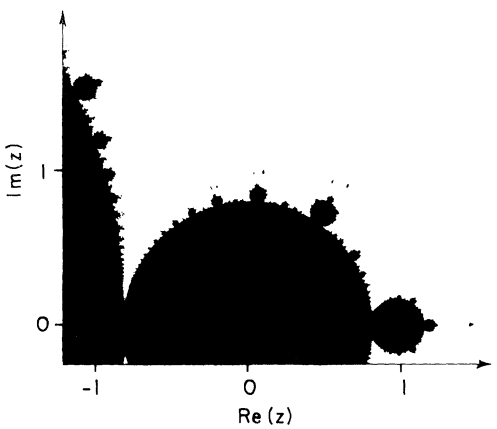

Fig. 6.1. Universal Mandelbrot cactus for the unstable manifold for $m/n=1/2$, obtained by iterating $g_{1/2}$ approximated by Table 6.4. As in Fig. 1.1, the black area represents values of the parameter p for which the iterates of the critical point $z=0$ do not tend to infinity. However, this is an enlargement of the asymptotic 2^∞ leaf of Fig. 1.1, so the cactus continues indefinitely to the left, each succeeding leaf larger by the factor $\delta=4.6692\ldots$

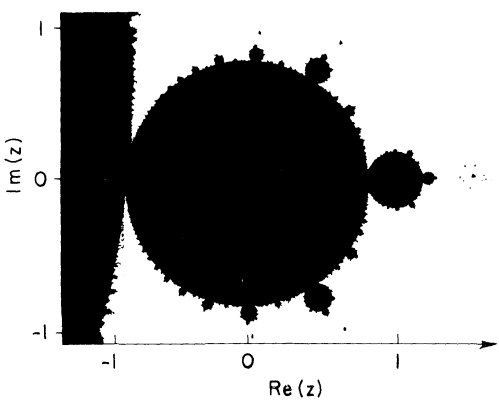

Fig. 6.2. Universal Mandelbrot cactus for $m/n=1/3$, obtained by iterating the unstable manifold universal function, Table 6.5. This is an enlargement of the asymptotic 3^∞ leaf of Fig. 1.1; the cactus winds indefinitely in a logarithmic spiral. The 1/3 cactus is slightly skew, unlike the 1/2 cactus which is symmetric across the real axis

Mandelbrot cactus; the radical difference is that they are infinite in extent. The "universal Julia sets" are also infinite in extent; by construction, $g_p(z)$ has infinitely many critical points, and each one has its own finite "universal basin of attraction," of the shape characteristic for the given cycle.

The first method for computing the scaling numbers, the universality equation (4.9), requires N-dimensional Newton-Raphson iteration, with quadratic convergence. The unstable manifold method (5.6) requires only one-dimensional Newton iteration, but also a parameterization by many more coefficients, of the order of N^2, and its convergence is only linear. In practice the first method is faster, but the second method yields not only the scaling numbers, but also an approximation to the unstable manifold which enables us to study the universal Mandelbrot cactuses.

The authors of [3] have noted that numerically the solutions of the universal equation (5.6) are stable under small non-analytic perturbations. Indeed, if we view the iteration space as a two-dimensional real space rather than a one-dimensional complex space, the convergence is controlled by the single unstable eigenvalue δ, regardless of whether the perturbations are analytic or not. However, even very small non-analytic perturbations cause drastic distortions of the leaves of the Mandelbrot cactus, destroying in the process the cactus-self-similarity, and with it the original rationale for formulating the universality equations. As we have argued in Sect. 2, analyticity is a crucial ingredient for the period n-tupling universality formulated in this article.

7. Discussion of Numerical Results

The self-similar structure of the Mandelbrot cactus, Fig. 1.1, suggests a systematic way of presenting the universal numbers that we have computed in the previous section. Observe that roughly halfway between any two large leaves on the periphery of a Mandelbrot cactus (such as 1/2 and 1/3) there is the next largest leaf (such as 2/5). Furthermore, we know from (4.6) that the size of the "cactus leaf" corresponding to period n-tupling is of order n^{-2}. Hence we need an interpolation scheme which organizes rational numbers m/n into self-similar levels of increasing period lengths n. Such a scheme is provided by Farey numbers [43, 44]. (The Farey tree is neither the only nor necessarily the best way of organizing rationals. One could instead, for example, partition rationals into continued fraction families. We have not attempted to apply other partitionings of rationals to this problem [45].)

Farey numbers are constructed by a simple interpolation rule: given two rationals m/n and m'/n', their Farey mediant is given by

$$m''/n'' = (m+m')/(n+n') . \tag{7.1}$$

Starting with the ends of the unit interval written as 0/1 and 1/1, this rule generates the Farey tree, Fig. 7.1.

Farey trees offer one way to encode the self-similarities of the Mandelbrot cactus. That might not be evident from the fractions listed in Fig. 7.1, but the following alternative construction of the Farey tree makes the self-similarities

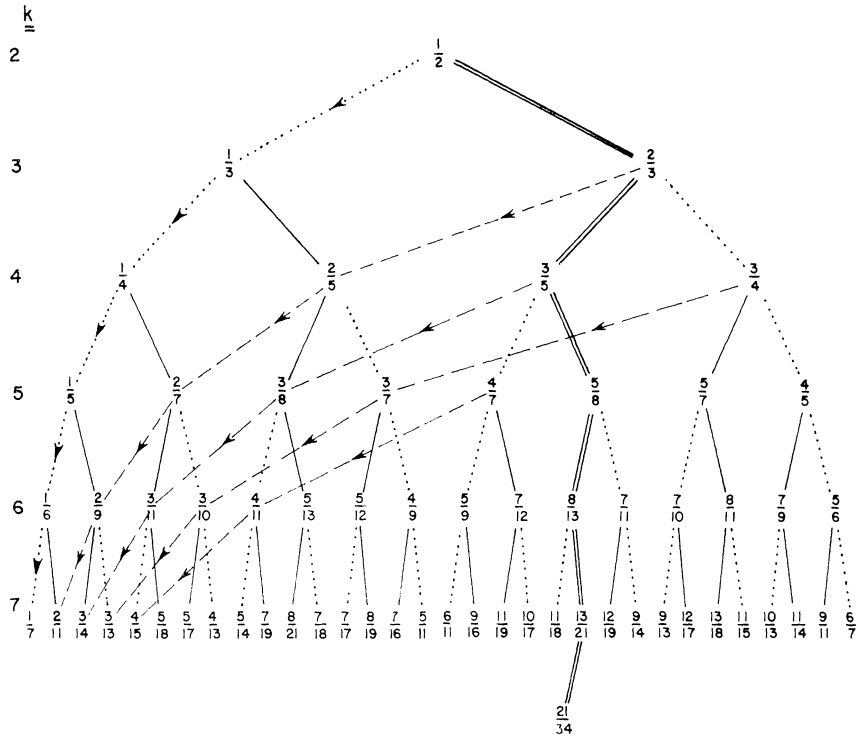

Fig. 7.1. The Farey tree. The double line indicates the Fibonacci sequence of rational approximations to the golden mean (more precisely to $1-\varrho$, with $\varrho=(1+\sqrt{5})/2$). The dashed lines are sequences of approximations to 0_+ of form m/∞

more explicit. Replace each Farey number by its continued fraction representation

$$m/n=[p_1,p_2,p_3,\ldots,p_k]=\cfrac{1}{p_1+\cfrac{1}{p_2+\cfrac{1}{p_3+\cfrac{1}{\ddots\cfrac{1}{p_k}}}}}$$

with p_i positive integers. The next level of the Farey tree is obtained by replacing the "last 1" in a continued fraction by either 2 or 1/2:

$$\begin{array}{ccc} & [p_1,p_2,\ldots,p_k,q] & \\ \swarrow & & \searrow \\ [p_1,p_2,\ldots,p_k,q+1] & & [p_1,p_2,\ldots,p_k,q-1,2] \end{array} \tag{7.3}$$

The resulting Farey tree is given in Fig. 7.2. The continued fraction representation shows explicitly that each branch of the Farey tree is similar to the entire tree, and suggests scaling laws for the associated universal numbers.

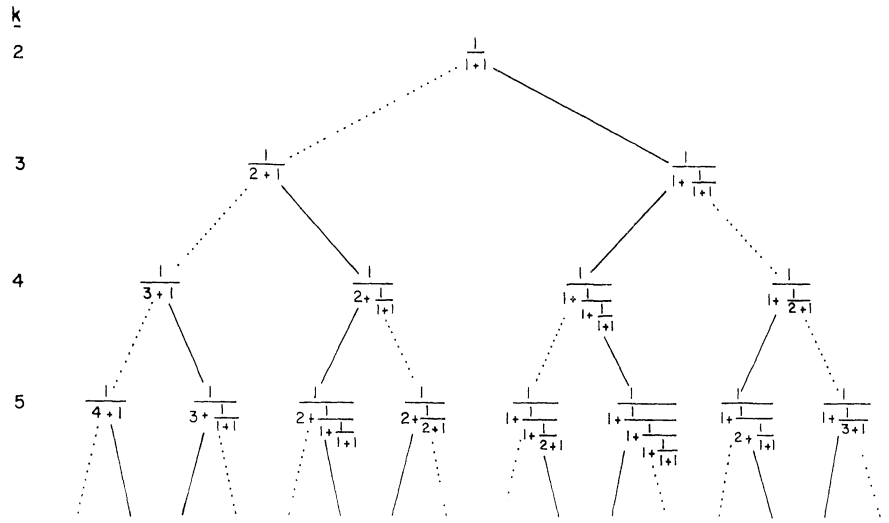

Fig. 7.2. A continued fraction representation of the Farey tree. The dotted and the full lines indicate substituting by 2 and 1/2, respectively

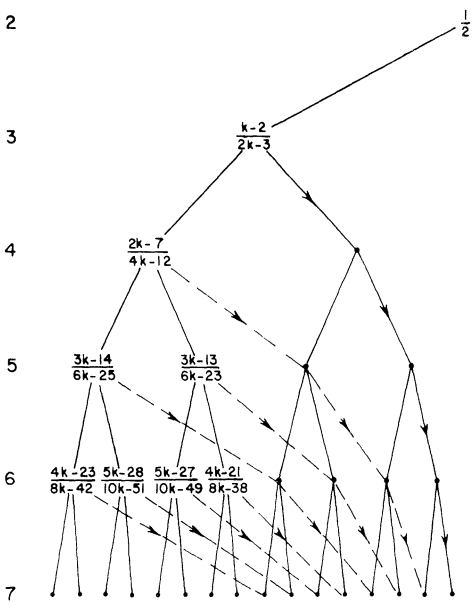

Fig. 7.3. Sequences of rational approximations to $1/2_-$ of form $1/(2+m/n)$, m fixed, $n\to\infty$

We have argued in Sect. 4 that α's and δ/n^2's for $1/n$ sequences, $n\to\infty$, converge to asymptotic limits. The Farey tree suggests two generalizations of this asymptotic behavior:

1. α, δ sequences for m/n, m fixed, $n\to\infty$, indicated by dashed lines in Fig. 7.1, should converge to asymptotic limits.

2. α, δ sequences for m/n, $n\to\infty$, $m/n\to P/Q$, P/Q any rational number, should converge to asymptotic limits. The dashed lines in Fig. 7.1 indicate sequences

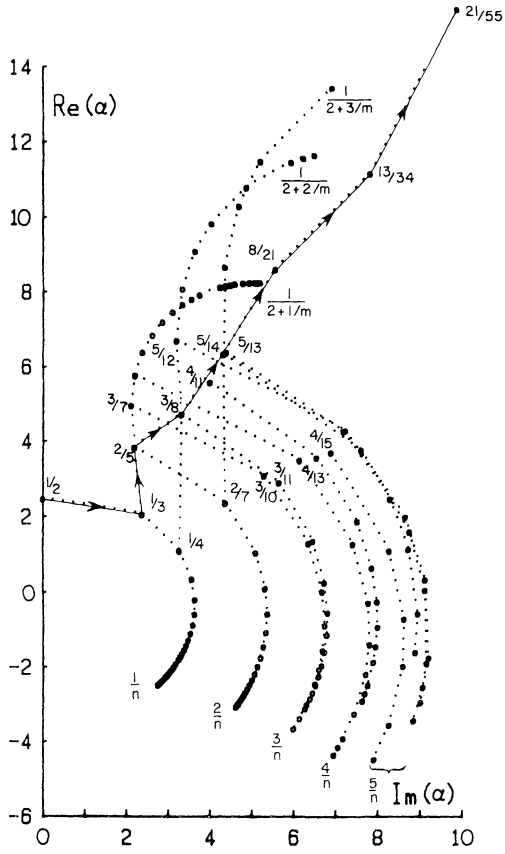

Fig. 7.4. The sequences of α's corresponding to rational approximations to 0_+ and $1/2_-$. The successive points in a sequence are connected by dotted lines, to guide the eye. The solid line indicates the Fibonacci sequence of rational approximations to the golden mean (more precisely to $1-\varrho$, with $\varrho=(1+\sqrt{5})/2$. The sequences of rational approximations to rationals accumulate at limit points in the complex plane. The Fibonacci sequences diverge in a controlled fashion (see text)

converging to $0/1_+$. Another example are sequences converging to $1/2_-$ indicated by dashed lines in Fig. 7.3.

The universal numbers corresponding to such sequences of Farey numbers are plotted in Figs. 7.4–7.9.

As argued in Sect. 4, the $\delta_{1/n}$'s have a simple asymptotic behavior as $n\to\infty$. This raises the hope that δ's (maybe even Feigenbaum's $\delta_{1/2}$) might be systematically calculable in an $1/n$ expansion. We have not attempted such calculation, but the discovery that large n limits are simple was the main motivation for the extensive numerical study of universal numbers presented here.

It is clear that sequences corresponding to approximations to different rational numbers, such as the 0_+ and the $1/2_-$ sequences, Fig. 7.4 and Fig. 7.5, are similar to each other, and that implicit in the Farey tree structure are scaling laws that relate the universal numbers [45].

There is one interesting example of such a scaling law, due to Manton and Nauenberg [5, 6]. While our universality generalizes period doublings, their universality generalizes the circle-map scaling of [18–20]. In this case one studies successive Fibonacci approximants to the golden mean winding number, and observes that the corresponding leaves of the Mandelbrot cactus are self-similar

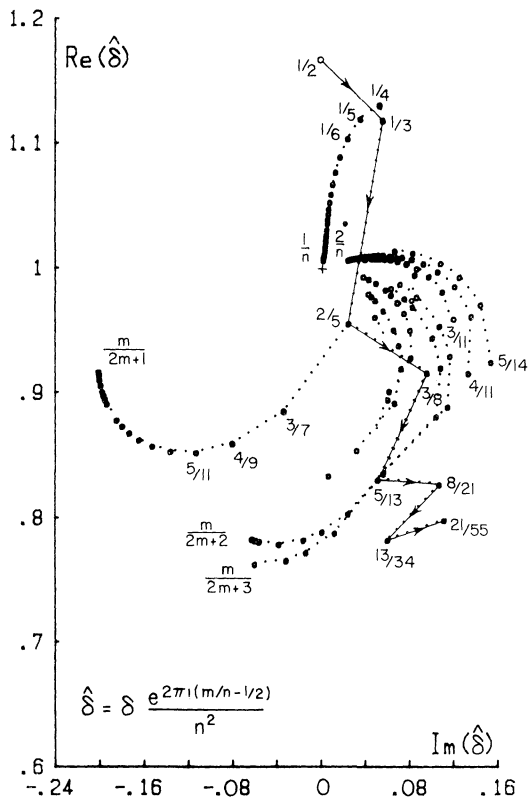

Fig. 7.5. The sequences of δ's corresponding to rational approximations to 0_+ and $1/2_-$. What is plotted is the ratio of δ and the conjectured asymptotic limit (4.6). 0_+ sequences appear to converge to the conjectured limit (marked by the cross)

under rescaling by the Manton-Nauenberg scaling number δ, and that the corresponding attractors are self-similar under rescaling by the Manton-Nauenberg α.

The Manton-Nauenberg scaling is an asymptotic scaling for our universal numbers in the following sense. From the construction of the unstable manifold (see Fig. 6.1 and Fig. 6.2) we know that $\delta_{m/n}$ measures the position of the center (the superstable value) of the m/n leaf of the corresponding universal cactus. If the universal cactuses for the consecutive ratios of Fibonacci numbers change

Fig. 7.6. The sequences of absolute values of α's corresponding to m/n, m fixed, $n\to\infty$ sequences of Farey numbers

Fig. 7.7. The sequences of absolute values of δ/n^2's corresponding to m/n, m fixed, $n\to\infty$ Farey sequences. According to the asymptotic conjecture (4.6), these sequences should converge to 1

Fig. 7.8. The deviation of the phase of $\delta=|\delta|\exp(2\pi i\theta)$ from the asymptotic estimate (4.6), $\Delta\theta=\theta+m/n-1/2$, for m/n, m fixed, $n\to\infty$ sequences

Fig. 7.9. The phase of $\alpha=|\alpha|\exp(2\pi i\theta)$ plotted as a deviation from its empirical limit, $\Delta\theta=\theta+3m/4n+1/8$, for m/n, m fixed, $n\to\infty$ sequences

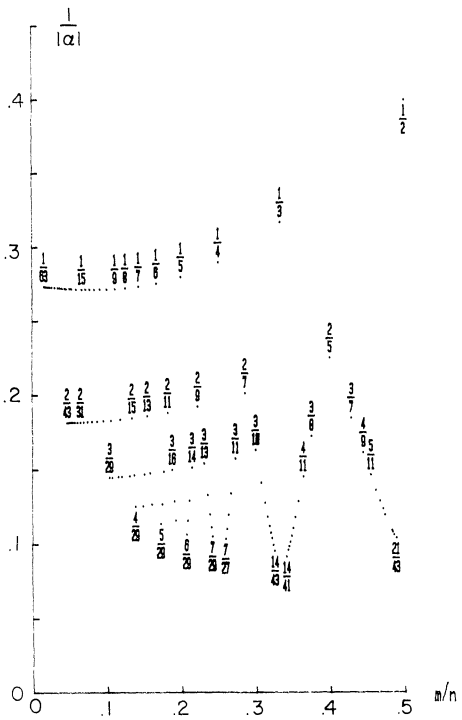

Fig. 7.6

Fig. 7.7

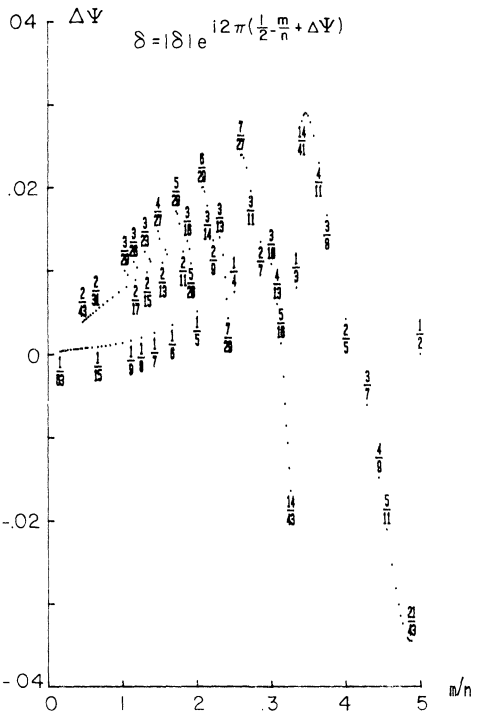

Fig. 7.8

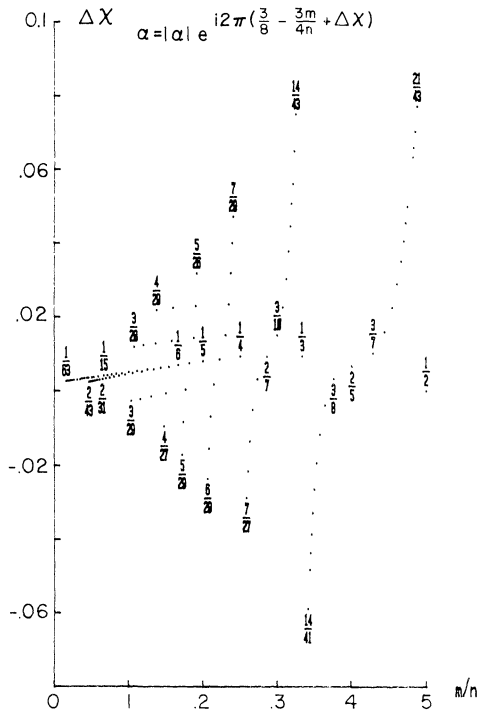

Fig. 7.9

smoothly, the Manton-Nauenberg δ is the limit of the ratio $(\delta_a - \delta_b)/(\delta_b - \delta_c)$, for a, b, c successive Fibonacci approximants to the golden mean.

Similarly, we know that inverse α's measure the distance by which the n^{th} iterate of the universal function misses the starting (i.e., the critical) point. This distance falls off rapidly for the cycles corresponding to the Fibonacci approximants to the golden mean (see Fig. 4.3), and the corresponding α's grow (see Fig. 7.4). The Manton-Nauenberg α is the limit of the ratio α_a/α_b for a, b successive ratios of Fibonacci numbers. For example, from our tables the absolute value of this ratio for $a = 34/55$, $b = 21/34$ is 0.74..., while the Manton-Nauenberg α is 0.7419.... The superstable trajectories for the successive Fibonacci approximants, Fig. 4.3, converge asymptotically to the fractal studied by Manton, Nauenberg and Widom.

While in the case of period n-tupling the conjectured universality is due to the infinite magnification of asymptotic cactuses, here the conjectured universality is due to the infinite magnification of the neighborhood of the golden mean winding number. Beyond these examples, there is infinity of other types of scaling laws hiding in the complex iterations. One can generalize Misiurewicz sequences [4], one can follow any sequence of islands (such as period triplings along the real axis) and so forth.

8. Summary

We have provided numerical evidence and heuristic arguments that the period-doubling universality generalizes to iterations of complex polynomials and polynomial-like mappings. This is summarized by the universal equations (4.9) and (5.6). We have solved these equations for a large number of different sequences of period n-tuplings; results of these numerical investigations are summarized by Table 6.1. The universal numbers can be organized by Farey numbers, Fig. 7.4 to Fig. 7.9.

Period doubling, the special case of the above theory, is an important route for transitions to chaos, observed experimentally in many different physical systems. Physical applications of complex universality are more uncertain. We do not know of a physical system modeled by complex iterations; as we argue in Sect. 2, we do not expect infinite sequences of period n-tuplings in a generic two-dimensional system. If such physical systems exist, experimental observation of sequences of period n-tuplings will be made difficult both by the n^4 reduction of the area in parameter space for each successive n-tupling, and by the $|\alpha|^2$ reduction of the basin of attraction, implying the need for very precise adjustment of initial conditions. The experimental precision for observing one period tripling is roughly the same as is required for observing two period doublings, so several period triplings could be observed.

Acknowledgements. We are grateful to Adrian Douady, Bodil Branner Jørgensen, J. Hamal Hubbard, Oscar Lanford, and Mitchell J. Feigenbaum for patient instruction.

Note to the revised manuscript. Since submission of this paper in January 1984 we have received a preprint by John Guckenheimer and Richard McGehee entitled "A proof of the Mandelbrot N^2 conjecture." The authors prove that the genericity assumption (3.4) and hence the relation (4.3) holds for the Fatou mapping (1.3).

References

1. Feigenbaum, M.J.: J. Stat. Phys. **19**, 25 (1978)
2. Feigenbaum, M.J.: J. Stat. Phys. **21**, 669 (1979)
3. Golberg, A.I., Sinai, Ya.G., Khanin, K.M.: Usp. Mat. Nauk **38**, 159 (1983)
4. Cvitanović, P., Myrheim J.: Phys. Lett. **94** A, 329 (1983)
5. Manton, N.S., Nauenberg, M.: Commun. Math. Phys. **89**, 555 (1983)
6. Widom, M.: Commun. Math. Phys. **92**, 121 (1983)
7. Collet, P., Eckmann, J.-P.: Iterated maps on interval as dynamical systems. Boston: Birkhäuser 1980
8. Cvitanović, P.: Acta Phys. Pol. A **65**, 203 (1984)
9. Cvitanović, P. (ed.): Universality in chaos. Bristol: Hilger 1984
10. Eckmann, J.-P.: Rev. Mod. Phys. **53**, 643 (1981)
11. Hu, B.: Phys. Rep. **91**, 233 (1982)
12. Hénon, M.: Commun. Math. Phys. **50**, 69 (1976)
13. Helleman, R.H.G., In: Fundamental problems in statistical mechanics, Vol. 5. Cohen, E.G.D. (ed.) Amsterdam: North-Holland 1980
14. Janssen, T., Tjon, J.A.: J. Phys. A **16**, 697 (1983)
15. Tomita, K.: Phys. Rep. **86**, 113 (1982)
16. D'Humieres, D., Beasley, M.R., Huberman, B.A., Libchaber, A.: Phys. Rev. A **26**, 3483 (1982)
17. For universality in hamiltonian period doublings see Green, J.M., MacKay, R.S., Vivaldi, F., Feigenbaum, M.J.: Physica **3** D, 468 (1981)
18. Shenker, S.J.: Physica **5** D, 405 (1982)
19. Feigenbaum, M.J., Kadanoff, L.P., Shenker, S.J.: Physica **5** D, 370 (1982)
20. Ostlund, S., Rand, D., Sethna, J., Siggia, E.D.: Physica D **8**, 303 (1983)
21. Physical applications of iterations of analytic maps have been discussed by Bessis, D., Geronimo, J.S., Moussa, P.: Saclay preprint SPhT/83/84
22. Fatou, P.: Bull. Soc. Math. France **47**, 161 (1919); ibid. **48**, 33 and 208 (1920)
23. Julia, G.: J. Math. Pures Appl. **4**, 47 (1918)
24. Lorenz, E.N.: Tellus **16**, 1 (1964)
25. May, R.M.: Nature **261**, 459 (1976)
26. Brooks, R., Matelski, J.P.: Proceedings of the 1978 Stony Brook Conference: Riemann Surfaces and related Topics. Ann. Math. Stud. **97**, 65 (1980); Mandelbrot, B.B.: Ann. N.Y. Acad. Sci. **357**, 249 (1980)
27. Mandelbrot, B.B.: The fractal geometry of nature. San Francisco: Freeman 1982
28. Douady, A., Hubbard, J.H.: C.R. Acad. Sci. Paris **294**, 123 (1982)
29. Douady, A.: Systemes dynamiques holomorphes, Seminaire Bourbaki 1982/83, No. 599
30. The connectedness of M has since also been proven by Sullivan, D.: IHES preprint M/83/1, (January 1982), in a more general setting
31. Douady and Hubbard have established this characterization for all connected components of the interior of M corresponding to attractive periodic orbits, as well as for some boundary points of M. It is an open problem whether the entire M can be characterized this way, see [29]
32. Grossmann, S., Thomae, S.: Z. Naturforsch. **32** A, 1353 (1977)
33. Schroeder, E.: Math. Ann. **3**, 296 (1871)
34. Siegel, C.L.: Ann. Math. **43**, 607 (1942)
35. This factor has been conjectured and numerically verified by Mandelbrot and collaborators (Mandelbrot, B.B.: private communication)
36. The geometrical problem is similar to the "Apollonian packing," the problem of covering a strip with non-overlapping disks
37. That the scaling is the consequence of the self-similarity of the Mandelbrot cactus was first conjectured by Mandelbrot, [27]
38. Cvitanović, P., Feigenbaum, M.J.: See [2]
39. Vul, E.B., Khanin, K.M.: Usp. Mat. Nauk. **37**, 173 (1982)
40. We are grateful to Feigenbaum, M.J. for teaching us how to compute with this method

41. A similar formulation of the universality theory (for the period doubling case) is due to Daido, H.: Phys. Lett. **86** A, 259 (1981); Prog. Theor. Phys. **67**, 1698 (1982)
42. This is essentially the same method as the one used by Feigenbaum [2] for solving the period-doubling $m/n = 1/2$ case
43. Hardy, G.H., Wright, E.M.: Theory of numbers, Oxford: Oxford University Press 1938
44. Allen, T.: Physica **6** D, 305 (1983)
45. There is a close analogy between δ's and the mode-locked intervals for circle maps. Scaling relations for mode-lockings are discussed in Cvitanović, P., Söderberg, B., Shraiman, B.: Physica Scripta **32**, 263 (1985)

Communicated by J.-P. Eckmann

Received February 27, 1984; in revised form November 24, 1987